PCCP

Cite this: *Phys. Chem. Chem. Phys.*, 2012, **14**, 5090–5099

www.rsc.org/pccp

DISCUSSION

New insights into the interface between a single-crystalline metal electrode and an extremely pure ionic liquid: slow interfacial processes and the influence of temperature on interfacial dynamics

Marcel Drüschler,[a] Natalia Borisenko,[b] Jens Wallauer,[a] Christian Winter,[a] Benedikt Huber,[a] Frank Endres[b] and Bernhard Roling*[a]

Received 7th December 2011, Accepted 3rd February 2012
DOI: 10.1039/c2cp40288b

Ionic liquids are of high interest for the development of safe electrolytes in modern electrochemical cells, such as batteries, supercapacitors and dye-sensitised solar cells. However, electrochemical applications of ionic liquids are still hindered by the limited understanding of the interface between electrode materials and ionic liquids. In this article, we first review the state of the art in both experiment and theory. Then we illustrate some general trends by taking the interface between the extremely pure ionic liquid 1-butyl-1-methylpyrrolidinium tris(pentafluoroethyl)trifluorophosphate and an Au(111) electrode as an example. For the study of this interface, electrochemical impedance spectroscopy was combined with *in situ* STM and *in situ* AFM techniques. In addition, we present new results for the temperature dependence of the interfacial capacitance and dynamics. Since the interfacial dynamics are characterised by different processes taking place on different time scales, the temperature dependence of the dynamics can only be reliably studied by recording and carefully analysing broadband capacitance spectra. Single-frequency experiments may lead to artefacts in the temperature dependence of the interfacial capacitance. We demonstrate that the fast capacitive process exhibits a Vogel–Fulcher–Tamman temperature dependence, since its time scale is governed by the ionic conductivity of the ionic liquid. In contrast, the slower capacitive process appears to be Arrhenius activated. This suggests that the time scale of this process is determined by a temperature-independent barrier, which may be related to structural reorganisations of the Au surface and/or to charge redistributions in the strongly bound innermost ion layer.

1. Introduction

In their recently published modern textbook "Interfacial Electrochemistry", W. Schmickler and E. Santos define electrochemistry as *the study of structures and processes at the interface between an electronic conductor* (*the electrode*) *and an ionic conductor* (*the electrolyte*) [...].[1] From this point of view, the electrochemistry of the electrode/ionic liquid interface is far away from being fully discovered, although various experimental techniques and computer simulation techniques have been employed within the last decade for probing this interface. To name just the most prominent ones, we mention high-energy X-ray reflectivity,[2,3] surface-enhanced Raman scattering (SERS),[4,5] sum-frequency generation vibrational spectroscopy (SFG),[6–10] *in situ* STM,[11–18] *in situ* AFM,[13,15,16,19–22] ac voltammetry,[23–28] electrochemical impedance spectroscopy (EIS)[29–43] as well as Monte Carlo and molecular dynamics simulations.[44–58] At the same time, theoreticians have taken first steps in the development of proper models for the potential-dependent structure of the interface between electrodes and dense ionic systems.[59–69]

In this article, we start with a description of the state of the art in this field. Then we review our recent experimental findings obtained by combining *in situ* STM, *in situ* AFM and EIS measurements for probing the interface between the extremely pure ionic liquid 1-butyl-1-methylpyrrolidinium tris(pentafluoroethyl)trifluorophosphate [$Py_{1,4}$][FAP] and a single-crystalline Au(111) surface. We consider this system as a well-suited model system. Subsequently, we present new results for the temperature dependence of the interfacial capacitance, and we compare our results to recently published data of other groups. We argue that the recording and the careful analysis of broadband capacitance spectra is a prerequisite for obtaining reliable data for the temperature dependence of the

[a] *Department of Chemistry, Philipps-University of Marburg, Hans-Meerwein-Straße, 35032 Marburg, Germany. E-mail: roling@staff.uni-marburg.de*
[b] *Institute of Particle Technology, Clausthal University of Technology, Arnold-Sommerfeld-Straße 6, 38678 Clausthal-Zellerfeld, Germany*

interfacial properties. In contrast, single-frequency measurements can easily lead to artefacts in the temperature dependence. Finally, we draw conclusions and give an outlook on directions for future work.

2. State of the art: recent experimental and theoretical work on the electrode/ionic liquid interface

(a) Oscillating ion layers and ordering phenomena

When bringing a charged or uncharged electrode surface in contact with an ionic liquid, several ion layers can be probed at the interface causing an oscillating charge density profile. The distance between the layers is close to the size of an ion pair.[2,3,13,15,16,19–22,42] This was first revealed by Atkin *et al.* using *in situ* AFM measurements for recording force–distance curves for ethylammonium nitrate, propylammonium nitrate and 1-ethyl-3-methylimidazolium acetate at mica, silica and graphite surfaces.[19] In recent papers, the same authors report on the first potential-dependent measurements of the force-separation profiles for $[Py_{1,4}]$FAP and 1-ethyl-3-methylimidazolium tris(pentafluoroethyl)trifluorophosphate, [EMIm][FAP], confined between Si_3N_4 tips and a single crystalline Au(111) surface.[15,16,22] Their results suggest that at the open circuit potential as well as at negative electrode potentials, the innermost layer is enriched with cations, while at positive electrode potentials, the anions are predominant in the innermost layer. Increasing the electrode potential generally increases the number of detectable ion layers and the force which is required to rupture them.

Here, we note that a potential-dependent structure consisting of alternating positively and negatively charged ion layers has already been discussed many years ago by Ukshe *et al.* and O. A. Esin[70–73] for the metal electrode/high-temperature molten salt interface. This observation has been explained by strong cation–anion correlations causing a so-called overscreening effect:[59,73–75] the innermost ion layer contains more charge than required for screening the charge of the electrode. Thus, the next ion layer has to exhibit an excess of co-charges, followed by a third ion layer with surplus counter-charges, and so on.

By using well-defined single crystalline metal electrodes, the potential dependent long-range restructuring of electrode surfaces as well as the formation of anion/cation adsorption layers have been directly observed by means of high-resolution *in situ* STM.[11–18] At cathodic potentials, the kinetically hindered formation of the herringbone reconstruction, Au(111)$(22 \times \sqrt{3})$, has been imaged for a single-crystalline Au(111) surface in contact with neat 1-butyl-3-methylimidazolium tetrafluoroborate $[BMIm][BF_4]$,[11] 1-butyl-3-methylimidazolium hexafluorophosphate $[BMIm][PF_6]$,[12] 1-butyl-1-methylpyrrolidinium bis[(trifluoromethyl)sulfonyl]amide $[Py_{1,4}][TFSA]$[13] and $[Py_{1,4}]$[FAP].[15]

Up to now, only Mao *et al.* have found a cation adsorption layer showing a well-ordered zig-zag-like super structure when they investigated the interface between $[BMIm][BF_4]$ and Au(100) at negative electrode potentials.[14] The authors emphasise that a structural commensurability between the unit cell of the ad-layer and the unit cell of single-crystalline electrode surface is a necessary condition, since cation adsorption of $[BMIm]^+$ in $[BMIm][BF_4]$ at Au(111) cannot be observed.[11,14] The formation of $[PF_6]^-$ anion adsorption layers showing a potential-dependent 2D phase transition from a moiré-like structure to a $(\sqrt{3} \times \sqrt{3})$ phase has been observed for $[BMIm][PF_6]$ at Au(111) by Pan and Freyland.[12] Similar observations have been published for the adsorption of $[BF_4]^-$ anions in $[BMIm][BF_4]$ at Au(100) by Mao *et al.*[14] However, the results of both groups are different from recently published results with extremely pure ionic liquids.[15–18] We would like to mention here that the interface ionic liquid/electrode is influenced by any kind of impurities. The addition of *e.g.* LiCl to $[Py_{1,4}]$[FAP] leads to attractive forces of the IL layers on the AFM cantilever instead of repulsive forces in the neat liquid.[16] Furthermore, the *in situ* STM images look different if LiCl is present, and we have hints that water also influences the interfacial structure. Thus, in order to comment reliably on interfacial processes in ionic liquids the quality of the liquid and its water content should be well known. Recently, Freire *et al.* showed that liquids with PF_6^- and BF_4^- ions are subject to hydrolysis, and liquids with the latter anion are never stable in the presence of water (neither during synthesis nor during experiments).[76] Consequently, the highest care is required in the interpretation of experiments at interfaces with such liquids, and in our opinion liquids of the highest available quality should be employed. Seddon *et al.* showed a few years ago that ionic liquids can in principle be distilled and that such thin films can be investigated by *e.g.* IR spectroscopy.[77,78] Souda and Steinrück *et al.* showed in parallel that highest-purity ionic liquid films can be prepared by evaporation/condensation in an ultrahigh vacuum, which is most likely the only way to make impurity free ionic liquids.[79,80]

We should also mention that even slight changes in the molecule structure of the ions will influence the interfacial structure. Therefore, the results from different liquids can deviate. Investigating the interfacial structure of $[Py_{1,4}]$[FAP] in contact with Au(111) by means of ultrahigh vacuum (UHV) STM, neither a well-ordered ad-layer structure could be obtained at room temperature nor could Au(111) be resolved atomically so far, although there was only one IL monolayer on top of the single crystalline gold surface.[17] It was concluded that the electrode/ion and ion/ion interaction is relatively weak and thus ions forming an ad-layer are rather mobile to an extent that a well-resolved image cannot be obtained. Decreasing the temperature to 210 K, the mobility was lowered and an ordered structure consisting of either ion pairs or distinct ions could be resolved.[17]

When probing the interface under electrochemical conditions in the anodic regime, very slow processes extending over hours were observed. These processes cause a formation of islands across the Au(111) surface.[16] The origin of these processes was attributed to kinetically hindered anion adsorption and desorption, which was also observed by Ouchi *et al.* at the interface between 1-butyl-3-methylimidazolium trifluoromethanesulfonate and a polycrystalline Pt electrode by means of SFG.[10]

In general, oscillating layers along the surface normal and complex 2D-structures across a section plane perpendicular to the surface normal[81] are caused by the concurrence of long-range Coulombic and short-range van der Waals interactions, as well as interionic dipole–dipole interactions and dipole–dipole interactions between the ions and the electrode.[21]

Finally, we note that Monte Carlo and molecular dynamics computer simulations also reveal the existence of oscillating ion density profiles at the electrode surface[44–58] and the formation of ion ad-layers[48,49,52,57] and thus confirm the experimental findings.

(b) Potential-dependent ion reorientation accompanied by charge redistribution

Using SERS and *in situ* AFM, it has been observed that the orientation of the ions within the first layers is very sensitive to the applied electrode potential and electrode charge, respectively.[5–10,15,16,22] For instance, the plane of the imidazolium ring at a [BMIm][PF_6]/Pt interface changes its orientation from 35° relative to the surface normal at a positive surface charge to 60° at a negative surface charge.[6] Potential-induced conformational and spatial reorientations of ions in the innermost layer of the interface have also been found in several simulations.[48,51,53–56,58] The reorientation process leads to charge redistributions, since voids are left behind when an ion changes its relative orientation from parallel to perpendicular. These voids can then be occupied by counter-ions.[51,54] The results of electrochemical impedance measurements suggest that these reorientations are slow, *i.e.* they take place on the time scale of seconds.[38,42]

(c) Potential-dependent differential interfacial capacitance

A fundamental property of the electrode/ionic liquid interface is the differential interfacial capacitance:[39,42,59,60]

$$C_{\mathrm{Int}} = \left.\frac{\partial q}{\partial(\Delta\varphi)}\right|_{\mu,T,p} \qquad (1)$$

Here, q denotes the electrode charge, while $\Delta\varphi$ is the potential difference between electrode and bulk of the ionic liquid. The differential interfacial capacitance is measured while keeping the chemical potential μ of the bulk ionic liquid, the temperature T and the pressure p constant. Electrochemical impedance spectroscopy is a powerful tool for measuring C_{Int} over a broad frequency range, thus probing the charge distribution at the interface over broad time scales.

We note that in the case of highly concentrated ionic systems, like ionic liquids, the differential interfacial capacitance cannot be described theoretically by the classical mean-field models, like *e.g.* the Stern model. These mean-field models neglect ion–ion and ion–electrode interactions. A first step towards more sophisticated theories is to take into account the finite volume of the ions, which limits their maximum concentration at the electrode surface. In 2007, Kornyshev presented a mean-field lattice gas model as one elegant way to do this.[59] Depending on the ion density, the model predicts either a global maximum of the differential interfacial capacitance at the potential of zero charge (PZC) or two maxima close to it. The drop of the differential capacitance with increasing electrode potential is caused by the entropy penalty for an accumulation of counter ions close to the charged surface. When the electrode potential is increased more and more, the electrode charge cannot be screened by a single layer of closely-packed counter-ions (lattice saturation). In this case, the layer has to grow in thickness causing a decay of the differential interfacial capacitance with $C_{\mathrm{Int}} \sim \Delta\varphi^{-1/2}$.

Ion–ion correlations and overscreening effects have been considered in several recent theoretical papers. For instance, Bazant *et al.* proposed that overscreening is only relevant at small potentials close to the PZC, whereas at higher potentials (more than ±2.5 V *versus* the PZC) lattice saturation is predominant.[66] In a MD simulation of the interface between 1-methyl-1-propylpyrrolidinium bis(fluorosulfonyl)imide, [$Py_{1,3}$][FSI] and graphite, Vatamanu *et al.*[56] have found that the transition from overscreening to lattice saturation extends over a much broader potential range than predicted by Bazant *et al.*[66] and that lattice saturation effects are not observable within the electrochemical stability window of the ionic liquid. In general, the potential dependence of the differential interfacial capacitance is mainly governed by the structure and dynamics of the first two or three ion layers adjacent to the electrode.

During the last decade, several groups have used ac voltammetry and EIS to measure the differential capacitance of various electrode/IL interfaces.[23–43] Despite a vast amount of experimental data, it is not easy to extract general trends from the data. Possible reasons for this were critically discussed by Lockett *et al.*,[37] who considered the ionic liquid purification procedure, the reference electrode stability, the surface of electrode materials and the methods for extracting capacitance data from EIS results.

Nevertheless, two trends in the experimental data are obvious. (i) The differential capacitance exhibits, in general, a weak dependence on the electrode potential, *i.e.* sharp features in potential-dependent capacitance curves are usually not observed.[15,39,42] This is in contrast to Kornyshev's mean-field lattice gas model. Here, the charge compensation in the double layer is governed by the entropy penalty for accumulating counter ions at the electrode, resulting in a quite strong dependence of the differential capacitance on the electrode potential.[59] On the other hand, the differential capacitance curves obtained in recent molecular dynamics simulations exhibit a weaker dependence on the electrode potential,[53,56] in agreement with experimental data. However, the underlying reason for this is not clear. (ii) The measured differential capacitance data show hysteresis effects, *i.e.* the values and shape of the potential-dependent capacitance curves depend on the potential scan direction.[30,33,36,39] These hysteresis effects are most likely related to slow interfacial processes.[15,33,39]

3. Experimental

Extremely pure, custom-made [$Py_{1,4}$][FAP] with all impurities guaranteed to be below 10 ppm was purchased from Merck KGaA. The so-obtained ionic liquid was dried for several hours under vacuum (10^{-3} mbar) at 100 °C in Clausthal and sent to Marburg in sealed ampoules. The ionic liquid was then stored in a glovebox with a high-purity N_2 atmosphere (LABstar, MBRAUN GmbH, H_2O and O_2 < 1 ppm). For the electrochemical measurements, a temperature-controlled microcell HC (rhd instruments) was used which was placed inside the glovebox. The measurements were carried out at temperatures ranging from 0 to 90 °C. Heating and cooling was done by means of a Peltier element with an accuracy of 0.01 °C. A three-electrode configuration was used for all measurements with a polycrystalline Pt disc (Goldschmiede Meusser, Marburg, Germany) acting as the counter electrode (CE), a mica-supported Au film with a

thickness of 200 nm (Agilent Technologies or phasis) acting as the working electrode (WE) and a Ag/Ag[TFSA]/[EMIm][TFSA]-based micro reference electrode (RE). The micro reference electrode consists of a Ag wire (99.999% from Alfa Aesar) in contact with a 100 mmol L^{-1} solution of Ag[TFSA] in [EMIm][TFSA].[82] To keep the ionic liquid in the measurement cell, a polyether ether ketone mould was clamped over a Viton O-ring onto the Au on mica substrate, resulting in a WE surface area of 0.38 cm^2. Directly before use, the Au film on mica substrates was carefully annealed for 30 s at 700 °C while being held under an Ar atmosphere or vacuum in a quartz tube. This ensures a better quality of the Au(111) surface, which had been epitaxially grown on mica during the production procedure,[83–85] and leads to much broader Au(111) terraces.[84] Furthermore, any possible surface contamination was minimised by the annealing process. The potential of the RE was tested and adjusted before and after each measurement against the ferrocene/ferricinium redox-couple, Fc^0/Fc^+, using a separate measurement setup and was found to be relatively stable over several weeks.[82]

The electrochemical measurement cell was connected to a Novocontrol modular measurement system consisting of an Alpha-AK high-resolution impedance analyser and a POT/GAL 15 V/10 A electrochemical interface. Before carrying out an EIS measurement, a cyclic voltammogram with a scan rate of 100 mV s^{-1} was recorded in order to determine the electrochemical window. Furthermore, the cyclic voltammogram is a fingerprint for the quality of the single-crystalline Au(111) surface. The EIS experiments were carried out at different WE dc potentials which were superimposed by a small ac voltage signal of $U_{ac,rms}$ = 10 mV. The frequency range typically extended from 10 mHz to 0.1 MHz. In the case of a single-frequency measurement, a frequency was chosen at which the phase angle was as close as possible to −90°. Usually after changing the temperature, the system was given an equilibration time of 10 min before starting a new EIS measurement. The recorded EIS data were fitted by means of the WinFit software (Novocontrol Technologies).

4. Review of recent results for the $[Py_{1,4}][FAP]$/Au(111) interface

The interface between extremely pure $[Py_{1,4}][FAP]$ and Au(111) was studied at room temperature by combining electrochemical impedance spectroscopy (Marburg group), *in situ* STM measurements (Clausthal group) and *in situ* AFM measurements (Atkin group, University of Newcastle, Australia).[15,16,42] In this section, we review the most important results for this model interface.

Fig. 1 represents a typical cyclic voltammogram of $[Py_{1,4}][FAP]$ in contact with freshly annealed Au(111) in a potential range extending from −2.3 to +1.2 V *versus* Fc^0/Fc^+. The temperature was kept at 20 °C and the scan rate was 100 mV s^{-1}. Except the first scan, the shape and the position of the current density features at potentials more positive than A_3 do not significantly alter, not even after several hours. However, the anodic current density peaks A_3^* and A_3 vanish after several cycles, while the current densities of C_2 and C_3 decrease significantly, pointing to slow processes which alter the electrode/ionic liquid interface.

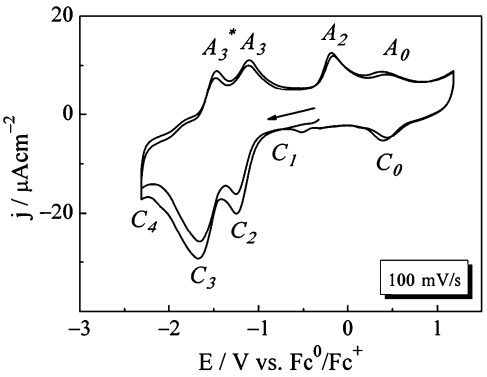

Fig. 1 A cyclic voltammogram of the interface between $[Py_{1,4}][FAP]$ and Au(111) measured at a scan rate of 100 mV s^{-1}. The first and second cycle are depicted.

(a) Cathodic scan direction

At least five cathodic processes are detectable within the chosen potential range (C_0–C_4). *In situ* STM has revealed that the Au(111) surface undergoes a herringbone reconstruction in the regime of C_1 and C_2, whereas the herringbone superstructure disappears at potentials around C_3.[15]

Fig. 2 shows the herringbone superstructure, and by comparison with literature results, the alternating fcc/hcp surface structures can be allocated. However, atomic resolution of Au(111) was not achieved, and the experiments presented in ref. 15 suggest that the observed structure is probed through a cation-rich layer. Results presented below support this interpretation.

In the more cathodic potential range, flat and uniform Au terraces were depicted (ref. 15) which obviously are also probed through a cation layer. Another cathodic process C_4, which is not clearly revealed in Fig. 1 due to the limited potential window of the measurement, has been attributed to the partial reduction of the $[Py_{1,4}]^+$ cation prior to decomposition.[15]

In situ AFM measurements within the cathodic potential regime (C_1–C_3) have indicated a strong interaction of the $[Py_{1,4}]^+$ cation with the Au(111) surface, so that the $[Py_{1,4}]^+$ cations predominantly populate the innermost ion layer. Sweeping the potential in the cathodic direction leads to an increase in the push-through forces and to a decrease of the

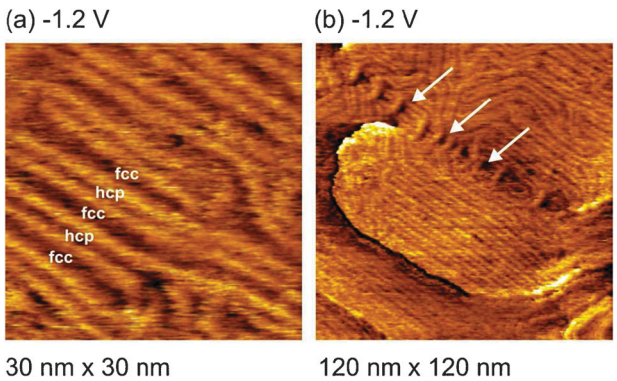

Fig. 2 The herringbone reconstruction of Au(111) in $[Py_{1,4}][FAP]$ (reprinted from ref. 15).

thickness of the innermost layer. This observation has pointed to an increase of the interaction forces and to a conformational change of the cations from an almost perpendicular orientation to the surface to a tilted or even parallel orientation.[15]

The results of EIS measurements provided information about the dynamics of interfacial processes. Three processes taking place on different time scales were observed.[15,42] The slowest process detectable at frequencies below 1 Hz seems to become faradaic in the low-frequency limit (impedance phase angle approaching 0°). The fastest process shows an almost ideal capacitive behaviour with a time scale in the millisecond regime. Such a time scale is expected for double layer formation governed by ion transport in the ionic liquid. In a potential range extending from C_1 to C_2, a second slower capacitive process was observed which is characterized by a time scale in the range of seconds.[15,42] Since the formation of the herringbone superstructure takes place in this potential range, the slow capacitive process was attributed to charge flow caused by the surface reconstruction.

In addition, we observed the ultra-slow formation of vacancies in the herringbone structure (in Fig. 3). This process could be responsible for the sub-Hz complex capacitance contribution probed by EIS. Depending on the applied electrode potential and depending on how long an electrode potential was applied, the herringbone structure either disappears rapidly or—with slightly different conditions—these vacancies grow, sometimes on the time scale of hours, sometimes within 10–15 min. A look at 5 year old *in situ* STM results of Au(111) under $[Py_{1,4}]$TFSA also gave hints for such vacancies in the herringbone structure, but we have not yet found such vacancies for Au(111) in [EMIm][TFSA], [EMIm][FAP] or [HMIm][FAP], where the herringbone structure either does not occur or needs other tunnelling parameters to be probed. If the electrode potential is increased, the vacancies disappear. As gold dissolution in this potential regime under a considerably strongly adsorbed cation layer is rather unlikely, there might either be an "underpotential" reduction of the $[Py_{1,4}]^+$ or trace amounts of *e.g.* water are reduced to hydrogen. Both *in situ* STM experiments with defined tiny amounts of water and electrochemical UHV-STM experiments would be suited to shed more light on this very slow process.

For a quantitative analysis of the capacitive processes, the broadband capacitance data were fitted to a Cole–Cole type expression:

$$(\hat{C}(\nu) - C_\infty) = \sum_{i=1}^{n} \frac{\Delta C_i}{1 + (j \cdot 2\pi\nu\tau_i)^{\alpha_i}} \qquad (2)$$

Here, C_∞ denotes the bulk capacitance, ν represents the frequency, and ΔC_i and τ_i are the capacitance relaxation strength and relaxation time of a process i, respectively, j denotes the imaginary unit, and α_i is a dimensionless value which contains information about the mechanism of the process.[39] The potential dependence of the capacitance relaxation strengths ΔC_1 (fast process) and ΔC_2 (slow process) were shown and discussed in refs 15 and 42.

(b) Anodic scan direction

Four oxidation peaks A_0, A_2, A_3 and A_3^* could be detected within the chosen potential window. A_2, A_3 and A_3^* seem to be correlated with the cathodic processes C_2 and C_3, since they only appear after the potentials of C_2 and C_3 have been reached.[15] Oxidation peak A_0 and the correlated reduction peak C_0 were only weakly pronounced during the first scan. They grow with increasing scan number, suggesting a gradual change of the interfacial structure. This finding was supported by *in situ* STM measurements starting from the open circuit potential and sweeping into the anodic direction. The recorded images revealed the potential-dependent formation of some islands across the surface.[16] This process was found to extend over time scales of several hours. Nevertheless, the process is reversible, *i.e.*, when the potential is swept back to the open circuit potential, the original Au(111) surface structure is recovered. Fig. 4 shows such an *in situ* STM image in the transition zone between cation and anion adsorption.

The *in situ* AFM measurements revealed similar trends as in the cathodic regime.[15,22] Anions are enriched in the innermost layer, and by increasing the anodic potential, the electrostatic interaction between the surface and the anions becomes stronger and causes an increase in the force required to disrupt the innermost layer. However, in contrast to the $[Py_{1,4}]^+$ cations, the $[FAP]^-$ anion cannot undergo significant conformational

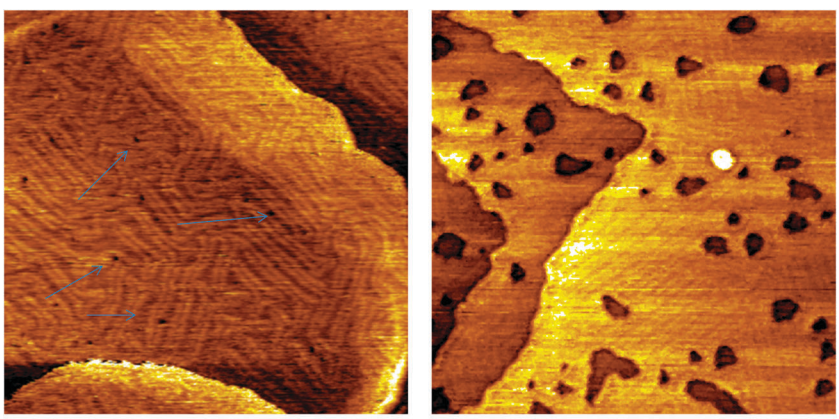

Fig. 3 Left: The herringbone reconstruction of Au(111) in $[Py_{1,4}][FAP]$; Right: vacancies form when the potential is shifted in the cathodic direction and/or when the interface is equilibrated over time scales of hours at cathodic potentials.

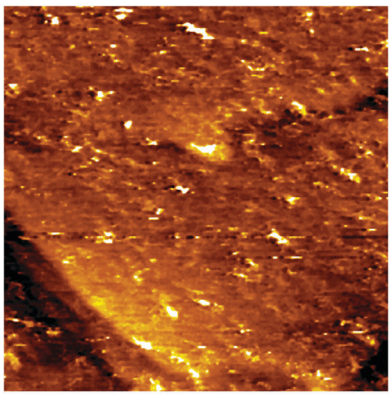

Fig. 4 An *in situ* STM image of $[Py_{1,4}][FAP]$ on Au(111) at anodic potentials (reprinted from ref. 16).

changes and thus the thickness of the innermost anion-enriched layer is not significantly influenced by the electrode potential.

EIS measurements at anodic potentials reveal three distinct processes as in the cathodic regime. Remarkably, a slow capacitive process is observable in the entire anodic regime.[42] This process was attributed to conformational changes of the cations leaving behind voids which are then occupied by anions. Since for this process to take place, interactions between the cations and the Au(111) surface have to be overcome, an additional activation energy for this process is expected which could be the reason for the longer time scale of this process. This type of process has also been found in recent simulation studies.[51,53,54,56]

5. Influence of temperature on the differential capacitance of the $[Py_{1,4}][FAP]$/Au(111) interface

In the following, we present new results for the influence of temperature on the differential capacitance of the $[Py_{1,4}][FAP]$/Au(111) interface. In a simple equivalent circuit, this interface can be modelled as a serial connection of an ohmic resistor R representing the ion transport in the ionic liquid and a capacitor C representing the electrochemical double layer.[39] In this circuit, the double layer charging time is $\tau = RC$. Since the ionic conductivity of ionic liquids increases with temperature, the resistance R and thus the time constant τ decrease with increasing temperature.[86–88] The time scale of the slower interfacial processes should also decrease with increasing temperature. Thus, processes being too slow at room temperature for being detected in the EIS frequency window should become observable at elevated temperatures. Moreover, the temperature dependence of the time constants should provide information about the activation energies of the processes.

In recent publications, it was claimed that the differential capacitance of IL/electrode interfaces increases with increasing temperature.[28–30,35,37] In contrast, most theoretical models developed so far predict either a general decrease of the differential interfacial capacitance with increasing temperature or a complicated behaviour with different potential ranges exhibiting different types of temperature dependences.[59,65] Lockett *et al.* proposed a model based on the weakening of coulombic interaction between ions forming stable ion pairs at elevated temperatures which leads to an increased availability of ions for storage at the electrode/ionic liquid interface.[30] Here, we show that a careful analysis of broadband capacitance spectra results in a very weak temperature dependence of the differential capacitance values. On the other hand, capacitance data recorded at a single frequency may pretend a strong temperature dependence, which is, however, an artefact due to the decrease of the time constants with increasing temperature.

In the following, we present the results of potential-dependent EIS measurements for the interface $[Py_{1,4}][FAP]$/Au(111) at temperatures ranging from 0 to 90 °C. A dc potential window extending from −1.14 to +0.56 V *versus* Fc^0/Fc^+ was chosen, since within this potential range mainly capacitive processes occur and thus the influence of irreversible faradaic processes during prolonged measurements is negligible. As the starting point, a WE potential of 0 V *versus* Fc^0/Fc^+ was selected. The potential was swept in steps of 20 mV in the anodic direction to +0.56 V *versus* Fc^0/Fc^+. Then the potential was swept to the cathodic limit −1.14 V *versus* Fc^0/Fc^+. At any potential, the full EIS spectrum was recorded for frequencies extending from 0.1 Hz to 0.1 MHz. After changing the temperature, the system was allowed to equilibrate for 10 min before the next measurement was started. An exemplary complex capacitance spectrum recorded at a WE potential of −0.9 V *versus* Fc^0/Fc^+ and a temperature of 20 °C is shown in Fig. 5 together with a fit to eqn (2). Two capacitive processes ($n = 1$ and 2) and a third ultraslow process ($n = 3$) are observed.

In Fig. 6, the relaxation strength of the fast capacitive process, ΔC_1, is plotted *versus* the WE potential. It is obvious that the differential capacitance shows a rather complicated potential and temperature dependence. However, at potentials more negative than 0 V *versus* Fc^0/Fc^+ there is a clear tendency that the differential capacitance decreases with increasing temperature.

For comparison, we show in Fig. 7 results for the real part of the capacitance obtained at a single frequency of 10 Hz. This frequency was chosen, since at room temperature (20 °C), the impedance phase angle is close to −90° (ideal capacitive behaviour). For these single-frequency measurements, a potential range from +0.18 V *versus* Fc^0/Fc^+ (open circuit potential) to −1.82 V *versus* Fc^0/Fc^+

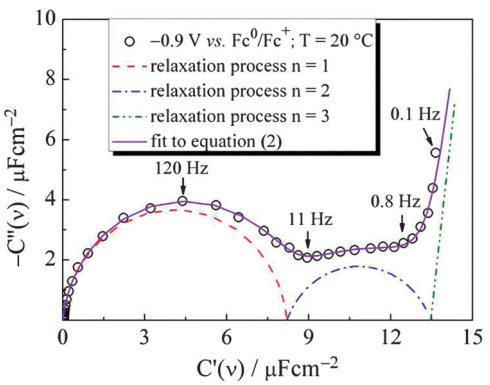

Fig. 5 Capacitance data of the interface between $[Py_{1,4}][FAP]$ and Au(111) at −0.9 V *versus* Fc^0/Fc^+ and at 20 °C (black circles). The violet line denotes a fit to eqn (2). The contributions of the different processes $n = 1$, 2 and 3 to the overall fit function are shown in red, blue and green.

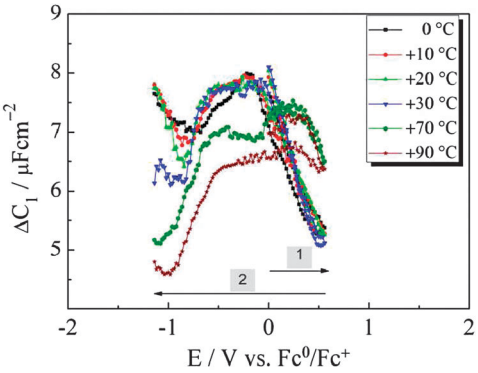

Fig. 6 The potential-dependent differential capacitance ΔC_1 of the fast capacitive process $n = 1$ at different temperatures.

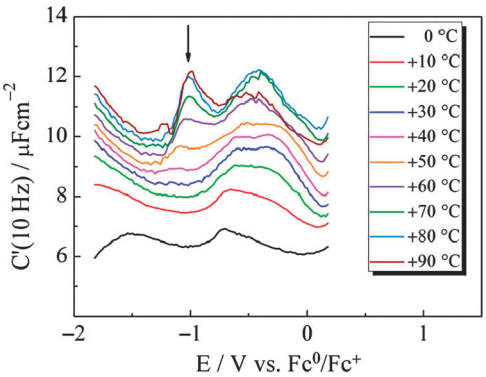

Fig. 7 The potential-dependence of C'(10 Hz) at different temperatures.

was chosen. Data were obtained in steps of 20 mV with a scan rate of approximately 100 mV s^{-1}.

The C'(10 Hz) data in Fig. 7 show a significant increase with increasing temperature, in agreement with previous studies.[28–30,35,37] However, this apparent increase is an artefact caused by the existence of different capacitive processes with temperature-dependent relaxation times. To demonstrate this, broadband capacitance data (0.1 MHz to 10 mHz) at a WE potential of −0.92 V *versus* Fc^0/Fc^+ are shown in Fig. 8 for several temperatures extending from 0 to 60 °C. The filled spheres mark the position of the data points obtained at 10 Hz.

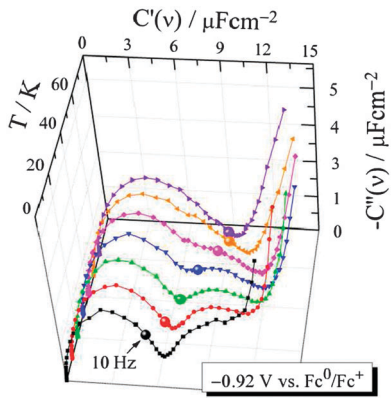

Fig. 8 A complex capacitance plane measured at −0.92 V *versus* Fc^0/Fc^+ and at 0, 10, 20, 30, 40, 50 and 60 °C.

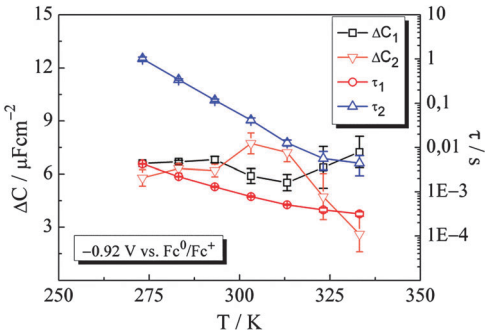

Fig. 9 Capacitance relaxation strengths for the fast and slow capacitive process, ΔC_1 and ΔC_2, as well as relaxation times τ_1 and τ_2 plotted *versus* temperature at a WE potential of −0.92 V *versus* Fc^0/Fc^+.

At 0 °C, the 10 Hz data point is part of the high-frequency semicircle due to the fast capacitive process, while at higher temperatures, the 10 Hz data become part of the second semicircle caused by the slower capacitive process. Consequently, the real part of the capacitance obtained at 10 Hz increases with increasing temperature. However, this does not mean that the relaxation strengths of the two capacitive processes increase with increasing temperature. A fit of the broadband capacitance data with eqn (2) results in relaxation strengths ΔC_1 and ΔC_2 and in relaxation times τ_1 and τ_2, which are plotted *versus* temperature in Fig. 9. While the relaxation strength ΔC_1 is virtually independent of temperature, the relaxation strength ΔC_2 seems to decrease at temperatures higher than 40 °C. However, this might be an artefact due to the strong overlap of the two semicircles at higher temperatures.

Furthermore, we would like to comment on the local maximum observable in the C'(10 Hz) data at temperatures above 50 °C (marked by an arrow in Fig. 7). Also this maximum is caused by the shift of the 10 Hz data from the high-frequency to the low-frequency semicircle at higher temperatures (Fig. 8) and is thus not a feature of the fast capacitive process. We conclude that single-frequency data are not well suited for a comprehensive analysis of the influence of temperature on the interfacial capacitance.

Finally, we consider the temperature dependence of the relaxation times τ_1 and τ_2. In Fig. 10, we show an Arrhenius plot of the relaxation times and of the ionic liquid conductivity.

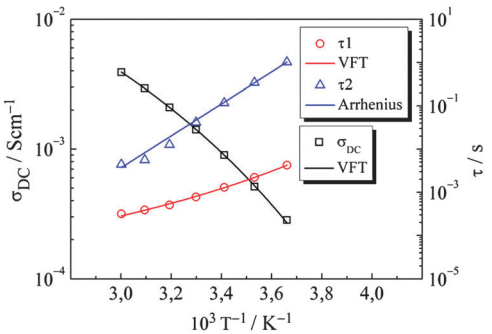

Fig. 10 The temperature dependence of the relaxation times τ_1 and τ_2 and of the ionic conductivity σ_{DC} at a WE potential of −0.92 V *versus* Fc^0/Fc^+.

Table 1 VFT and Arrhenius parameters of capacitance relaxation times and ionic conductivity

$\tau_1 = \tau_1^* \exp[A_1/(T - T_1)]$			$\tau_2 = \tau_2^* \exp(\varepsilon_A/kT)$	
τ_1^*/μs	A_1/K	T_1^*/K	τ_2^*/fs	ε_A/eV
3.1 ± 1.8	723 ± 128	173 ± 10	28 ± 8	0.738 ± 0.007
$\chi^2 = 7.92 \times 10^{-10}$	$R = 0.99961$		$\chi^2 = 2.33 \times 10^{-5}$	$R = 0.99983$
$\tau_2 = \tau_2^* \exp[A_2/(T - T_2)]$				
τ_2^*/μs		A_2/K	T_2/K	
0.59 ± 3.15		1680 ± 1281	156 ± 46	
$\chi^2 = 1.79 \times 10^{-4}$			$R = 0.99870$	
$\sigma_{DC} = \sigma_0 \exp[-B/(T - T_0)]$				
σ_0/Scm^{-1}		B/K	T_0/K	
0.26 ± 0.04		644 ± 46	179 ± 5	
$\chi^2 = 1.25 \times 10^{-10}$			$R = 0.99993$	

As expected, both the ionic conductivity σ_{DC} and the relaxation time τ_1 exhibit a Vogel–Fulcher–Tamann-type (VFT-type) temperature dependence:[86–91]

$$\tau_1 = \tau_1^* \exp[A_1/(T - T_1)] \quad (3a)$$

$$\sigma_{DC} = \sigma_0 \exp[-B/(T - T_0)] \quad (3b)$$

For analysing the temperature dependence of the relaxation time of the slower capacitive process, τ_2, we carried out comparative VFT and Arrhenius fits:

$$\tau_2 = \tau_2^* \exp(\varepsilon_A/kT) \quad (3c)$$

$$\tau_2 = \tau_2^* \exp[A_2/(T - T_2)] \quad (3d)$$

In eqns (3a)–(3d), τ_1^*, A_1, T_1, τ_2^*, ε_A, T_2, σ_{DC}, σ_0, B and T_0 are adjustable parameters. The best-fit parameters are summarised in Table 1.

In the case of the relaxation time τ_2, a better fit was obtained when the Arrhenius law, eqn (3c), was used. It is important to note that due to the relatively large errors of τ_2 at high temperatures, the outcome of the fit cannot be considered as proof for an Arrhenius-type temperature dependence of τ_2, but only as an indication.

In Fig. 11, we show Arrhenius plots of the ionic conductivity multiplied by the relaxation time τ_1 and by the relaxation time τ_2, respectively. The product $\sigma_{DC}\cdot\tau_1$ exhibits no significant temperature dependence indicating that the time scale of the fast process is governed by the ionic conductivity. In contrast, the product $\sigma_{DC}\cdot\tau_2$ depends strongly on temperature. This shows that the time scale of the slow capacitive process is not determined by ion transport in the ionic liquid. The Arrhenius fit of τ_2 suggests that the slow process is characterised by a temperature-independent activation barrier, which may reflect a barrier for the reconstruction of the electrode surface and/or a barrier for the reorientation of strongly bound ions in the innermost layer.

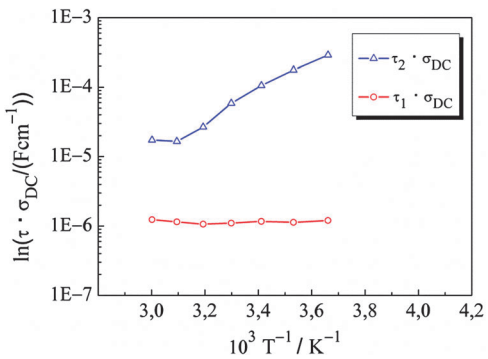

Fig. 11 The temperature dependence of $\sigma_{DC}\cdot\tau$ for τ_1 and τ_2 at a WE potential of −0.92 V *versus* Fc^0/Fc^+.

6. Summary and outlook

The *in situ* STM, *in situ* AFM and EIS results summarised in this article clearly reveal that the understanding of the structure and dynamics of the ionic liquid/electrode interface is indeed a challenging task. EIS measurements probe two distinct capacitive processes taking place on different time scales. The time scale of the fast capacitive process exhibits virtually the same VFT-type temperature dependence as the bulk conductivity of the ionic liquid. Thus, this process can be identified with double layer formation governed by ion transport in the ionic liquid. The slow process exhibits a time scale of seconds at room temperature. Comparative VFT and Arrhenius fits for the temperature dependence of the time scale indicate an Arrhenius-type temperature dependence. This suggest that the slow process is caused by temperature-independent activation barriers, most likely barriers for the reconstruction of the electrode surface and/or barriers for the reorientation of strongly bound ions in the innermost layer.

The differential capacitance of both capacitive processes shows a tendency to decrease with increasing temperature. The apparent increase of the differential capacitance with increasing temperature found in single-frequency measurements appears to be an artefact due to the existence of two capacitive processes with temperature-dependent relaxation times.

In addition, a third ultraslow process is probed by EIS, which might be related to ultraslow vacancy formation in the Au surface observed by *in situ* STM measurements. The origin of this process still needs to be investigated in more detail.

In situ STM measurements are well suited for the investigation of electrodes in contact with ionic liquids. A typical tunneling distance is between 1 and 2 nm, thus up to 3 layers can be probed by STM. As the interface electrode/ionic liquid is affected by impurities,

and in this context we even regard water as an impurity, one has to take care with the interpretation of STM images and at least the quality of the liquids with the detected impurities should be stated. For electrochemical application, lithium salts, solutes, additives and possibly water may be added to the ionic liquid and therefore it will be worth investigating how the interfacial structure is then altered.

In situ AFM measurements reveal the existence of several ion layers bound to the electrode surface. In general, the number of layers and the forces required to rupture them increases with increasing electrode potential. This *in situ* technique will also provide valuable information about the influence of lithium salts, solutes, additives and water on the structure of the interfacial layer.

The interface between ionic liquids and other types of electrode materials should also be investigated in more detail. Examples are electrodes based on graphene,[92–96] on meso- and nanoporous carbons[97–102] and on porous oxides.[103–105] Electrochemical impedance spectra of such ionic liquid/electrode interfaces point to the existence of more than one capacitive process.[92,96,97,100] Since in the case of porous electrodes, *in situ* STM and AFM techniques are not easily applicable, alternative methods, such as quartz microbalance measurements[106] and *in situ* NMR techniques,[107] should be also combined with EIS measurements.

Acknowledgements

This work was financially supported by the Deutsche Forschungsgemeinschaft (DFG) within the Priority Program SPP 1191 (Ionic Liquids), and by the Fonds der Chemischen Industrie (FCI; PhD stipend for M. D.).

References

1 W. Schmickler and E. Santos, *Interfacial Electrochemistry*, Springer-Verlag, Berlin Heidelberg, 2nd edn, 2010.
2 M. Mezger, H. Schröder, H. Reichert, S. Schramm, J. S. Okasinski, S. Schöder, V. Honkimäki, M. Deutsch, B. M. Ocko, J. Ralston, M. Rohwerder, M. Stratmann and H. Dosch, *Science*, 2008, **322**, 424.
3 M. Mezger, S. Schramm, H. Schröder, H. Reichert, M. Deutsch, E. J. De Souza, J. S. Okasinski, B. M. Ocko, V. Honkimäki and H. Dosch, *J. Chem. Phys.*, 2009, **131**, 094701.
4 V. O. Santos Jr., M. B. Alves, M. S. Carvalho, P. A. Z. Suarez and J. C. Rubim, *J. Phys. Chem. B*, 2006, **110**, 20379.
5 Y. X. Yuan, T. C. Niu, M. M. Xu, J. L. Yao and R. A. Gu, *J. Raman Spectrosc.*, 2009, **41**, 516.
6 S. Rivera-Rubero and S. Baldelli, *J. Phys. Chem. B*, 2004, **108**, 15133.
7 S. Baldelli, *J. Phys. Chem. B Lett.*, 2005, **109**, 13049.
8 C. Aliaga and S. Baldelli, *J. Phys. Chem. B*, 2006, **110**, 18481.
9 S. Baldelli, *Acc. Chem. Res.*, 2008, **41**, 421.
10 W. Zhou, S. Inoue, T. Iwahashi, K. Kanai, K. Seki, T. Miyamae, D. Kim, Y. Katayama and Y. Ouchi, *Electrochem. Commun.*, 2010, **12**, 672.
11 L. G. Lin, Y. Wang, J. W. Yan, Y. Z. Yuan, J. Xiang and B. W. Mao, *Electrochem. Commun.*, 2003, **5**, 995.
12 G.-B. Pan and W. Freyland, *Chem. Phys. Lett.*, 2006, **427**, 96.
13 R. Atkin, S. Z. El Abedin, R. Hayes, L. H. S. Gasparotto, N. Borisenko and F. Endres, *J. Phys. Chem. C*, 2009, **113**, 13266.
14 Y. Z. Su, Y. C. Fu, J. W. Yan, Z. B. Chen and B. W. Mao, *Angew. Chem.*, 2009, **121**, 5250.
15 R. Atkin, N. Borisenko, M. Drüschler, S. Z. El Abedin, F. Endres, R. Hayes, B. Huber and B. Roling, *Phys. Chem. Chem. Phys.*, 2011, **13**, 6849.
16 F. Endres, N. Borisenko, S. Z. El Abedin, R. Hayes and R. Atkin, *Faraday Discuss.*, 2012, **154**, 221.
17 T. Waldmann, H. Huang, H. E. Hoster, O. Höfft, F. Endres and R. J. Behm, *ChemPhysChem*, 2011, **12**, 2565.
18 N. Borisenko, S. Z. El Abedin and F. Endres, *ChemPhysChem*, 2012, DOI: 10.1002/cphc.201100873.
19 R. Atkin and G. G. Warr, *J. Phys. Chem. C*, 2007, **111**, 5162.
20 R. Hayes, S. Z. El Abedin and R. Atkin, *J. Phys. Chem. B*, 2009, **113**, 7049.
21 R. Hayes, G. G. Warr and R. Atkin, *Phys. Chem. Chem. Phys.*, 2010, **12**, 1709.
22 R. Hayes, N. Borisenko, M. K. Tam, P. C. Howlett, F. Endres and R. Atkin, *J. Phys. Chem. C*, 2011, **115**, 6855.
23 C. Nanjundiah, S. F. McDevitt and V. R. Koch, *J. Electrochem. Soc.*, 1997, **144**, 3392.
24 M. T. Alam, Md. M. Islam, T. Okajima and T. Ohsaka, *J. Phys. Chem. C*, 2007, **111**, 18326.
25 M. T. Alam, Md. M. Islam, T. Okajima and T. Ohsaka, *J. Phys. Chem. C*, 2008, **112**, 2601.
26 Md. M. Islam, M. T. Alam and T. Ohsaka, *J. Phys. Chem. C*, 2008, **112**, 16568.
27 M. T. Alam, Md. M. Islam, T. Okajima and T. Ohsaka, *J. Phys. Chem. C*, 2008, **112**, 16600.
28 M. T. Alam, J. Masud, Md. M. Islam, T. Okajima and T. Ohsaka, *J. Phys. Chem. C*, 2011, **115**, 19797.
29 F. Silva, C. Gomes, M. Figueiredo, R. Costa, A. Martins and C. M. Pereira, *J. Electroanal. Chem.*, 2008, **622**, 153.
30 V. Lockett, R. Sedev, J. Ralston, M. Horne and T. Rodopoulos, *J. Phys. Chem. C*, 2008, **112**, 7486.
31 J. P. Zheng, P. C. Goonetilleke, C. M. Pettit and D. Roy, *Talanta*, 2010, **81**, 1045.
32 M. Gnahm, T. Pajkossy and D. M. Kolb, *Electrochim. Acta*, 2010, **55**, 6212.
33 M. Drüschler, B. Huber, S. Passerini and B. Roling, *J. Phys. Chem. C*, 2010, **114**, 3614.
34 L. Siinor, K. Lust and E. Lust, *J. Electrochem. Soc.*, 2010, **157**, F83.
35 R. Costa, C. M. Pereira and F. Silva, *Phys. Chem. Chem. Phys.*, 2010, **12**, 11125.
36 R. T. Gore, T. Bond, W. Zhang, R. W. J. Scott and I. Burgess, *Electrochem. Commun.*, 2010, **12**, 1340.
37 V. Lockett, M. Horne, R. Sedev, T. Rodopoulos and J. Ralston, *Phys. Chem. Chem. Phys.*, 2010, **12**, 12499.
38 T. Pajkossy, *Pure Appl. Chem.*, 2011, **83**, 259.
39 M. Drüschler, B. Huber and B. Roling, *J. Phys. Chem. C*, 2011, **115**, 6802.
40 T. Pajkossy and D. M. Kolb, *Electrochem. Commun.*, 2011, **13**, 284.
41 M. Gnahm, C. Müller, R. Répánszki, T. Pajkossy and D. M. Kolb, *Phys. Chem. Chem. Phys.*, 2011, **13**, 11627.
42 B. Roling, M. Drüschler and B. Huber, *Faraday Discuss.*, 2012, **154**, 303.
43 Y. Z. Su, Y. C. Fu, Y. M. Wie, J. W. Yan and B. W. Mao, *ChemPhysChem*, 2010, **11**, 2764.
44 S. K. Reed, O. J. Lanning and P. A. Madden, *J. Chem. Phys.*, 2007, **126**, 084704.
45 M. V. Fedorov and A. A. Kornyshev, *Electrochim. Acta*, 2008, **53**, 6835.
46 M. V. Fedorov and A. A. Kornyshev, *J. Phys. Chem. B Lett.*, 2008, **112**, 11868.
47 G. Feng, J. S. Zhang and R. Qiao, *J. Phys. Chem. C*, 2009, **113**, 4549.
48 S. A. Kislenko, I. S. Samoylov and R. H. Amirov, *Phys. Chem. Chem. Phys.*, 2009, **11**, 5584.
49 M. Pounds, S. Tazi and P. A. Madden, *J. Phys.: Condens. Matter*, 2009, **21**, 424109.
50 S. Wang, S. Li, Z. Cao and T. Yan, *J. Phys. Chem. C*, 2010, **114**, 990.
51 M. V. Fedorov, N. Georgi and A. A. Kornyshev, *Electrochem. Commun.*, 2010, **12**, 296.
52 S. Tazi, M. Salanne, C. Simon, P. Turq, M. Pounds and P. A. Madden, *J. Phys. Chem. B*, 2010, **114**, 8453.
53 J. Vatamanu, O. Borodin and G. D. Smith, *J. Am. Chem. Soc.*, 2010, **132**, 14825.
54 N. Georgi, A. A. Kornyshev and M. V. Fedorov, *J. Electroanal. Chem.*, 2010, **649**, 261.
55 G. Feng, R. Qiao, J. Huang, S. Dai, B. G. Sumpter and V. Meunier, *Phys. Chem. Chem. Phys.*, 2011, **13**, 1152.

56 J. Vatamanu, O. Borodin and G. D. Smith, *J. Phys. Chem. B*, 2011, **115**, 3073.
57 C. Merlet, M. Salanne, B. Rotenberg and P. A. Madden, *J. Phys. Chem. C*, 2011, **115**, 16613.
58 A. I. Frolov, K. Kirchner, T. Kirchner and M. V. Fedorov, *Faraday Discuss.*, 2012, **154**, 235.
59 A. A. Kornyshev, *J. Phys. Chem. B*, 2007, **111**, 5545.
60 K. B. Oldham, *J. Electroanal. Chem.*, 2008, **613**, 131.
61 Y. Lauw, M. D. Horne, T. Rodopoulos and F. A. M. Leermakers, *Phys. Rev. Lett.*, 2009, **103**, 117801.
62 Y. Lauw, M. D. Horne, T. Rodopoulos, A. Nelson and F. A. M. Leermakers, *J. Phys. Chem. B*, 2010, **114**, 11149.
63 W. R. Fawcett and P. J. Ryan, *Phys. Chem. Chem. Phys.*, 2010, **12**, 9816.
64 M. S. Loth, B. Skinner and B. I. Shklovskii, *Phys. Rev. E: Stat., Nonlinear, Soft Matter Phys.*, 2010, **82**, 016107.
65 M. S. Loth, B. Skinner and B. I. Shklovskii, *Phys. Rev. E: Stat., Nonlinear, Soft Matter Phys.*, 2010, **82**, 056102.
66 M. Z. Bazant, B. D. Storey and A. A. Kornyshev, *Phys. Rev. Lett.*, 2011, **106**, 046102.
67 D. Henderson and S. Lamperski, *J. Chem. Eng. Data*, 2011, **56**, 1204.
68 D. Jian, D. Meng and J. Wu, *Chem. Phys. Lett.*, 2011, **504**, 153.
69 J. Forsman, C. E. Woodward and M. Trulsson, *J. Phys. Chem. B*, 2011, **115**, 4606.
70 E. A. Ukshe, N. G. Bukun, D. I. Leikis and A. N. Frumkin, *Electrochim. Acta*, 1964, 431.
71 O. A. Esin, *Zh. Fiz. Khim.*, 1956, **30**, 3.
72 A. D. Graves, *J. Electroanal. Chem.*, 1970, **25**, 349.
73 A. D. Graves and D. Inman, *J. Electroanal. Chem.*, 1970, **25**, 357.
74 M. Rovere and M. P. Tosi, *Rep. Prog. Phys.*, 1986, **49**, 1001.
75 Y. Levin, *Rep. Prog. Phys.*, 2002, **65**, 1577.
76 M. G. Freire, C. M. S. S. Neves, I. M. Marrucho, J. A. P. Coutinho and A. M. Fernandes, *J. Phys. Chem. A*, 2010, **114**, 3744.
77 M. J. Earle, J. M. S. S. Esperanca, M. A. Gilea, J. N. C. Lopes, L. P. N. Rebelo, J. W. Magee, K. R. Seddon and J. A. Widegren, *Nature*, 2006, **439**, 831.
78 D. H. Zaitsau, G. J. Kabo, A. A. Strechan, Y. U. Paulechka, A. Tschersich, S. P. Verevkin and A. Heintz, *J. Phys. Chem. A*, 2006, **110**, 7303.
79 R. Souda, *J. Phys. Chem. B*, 2008, **112**, 15349.
80 T. Cremer, M. Killian, J. M. Gottfried, N. Paape, P. Wasserscheid, F. Maier and H.-P. Steinrueck, *ChemPhysChem*, 2008, **9**, 2185.
81 K. Shimizu, A. Pensado, P. Malfreyt, A. A. H. Pádua and J. N. C. Lopes, *Faraday Discuss.*, 2012, **154**, 155.
82 B. Huber and B. Roling, *Electrochim. Acta*, 2011, **56**, 6569.
83 K. Müller and H. Viefhaus, *Z. Naturforschg.*, 1966, **21a**, 1726.
84 H. Viefhaus, *Z. Naturforschg.*, 1967, **22a**, 2123.
85 M. Levlin, A. Laakso, H. E. M. Niemi and P. Hautojärvi, *Appl. Surf. Sci.*, 1997, **115**, 31.
86 H. Tokuda, K. Hayamizu, K. Ishii, Md. Abu Bin Hasan Susan and M. Watanabe, *J. Phys. Chem. B*, 2004, **108**, 16593.
87 H. Tokuda, K. Hayamizu, K. Ishii, Md. Abu Bin Hasan Susan and M. Watanabe, *J. Phys. Chem. B*, 2005, **109**, 6103.
88 H. Tokuda, K. Ishii, Md. Abu Bin Hasan Susan, S. Tsuzuki and M. Watanabe, *J. Phys. Chem. B*, 2006, **110**, 2833.
89 H. Vogel, *Phys. Z.*, 1921, **22**, 645.
90 G. S. Fulcher, *J. Am. Ceram. Soc.*, 1925, **8**, 339.
91 G. Tamman and W. Hesse, *Z. Anorg. Allg. Chem.*, 1926, **156**, 245.
92 J. R. Miller, R. A. Outlaw and B. C. Holloway, *Science*, 2010, **329**, 1637.
93 D. A. C. Brownson, D. K. Kampouris and C. E. Banks, *J. Power Sources*, 2011, **196**, 4873.
94 Z. Lin, Y. Liu, Y. Yao, O. J. Hildreth, Z. Li, K. Moon and C. Wong, *J. Phys. Chem. C*, 2011, **115**, 7120.
95 X. Yang, J. Zhu, L. Qiu and D. Li, *Adv. Mater.*, 2011, **23**, 2833.
96 Y. Zhu, S. Murali, M. D. Stoller, K. J. Ganesh, W. Cai, P. J. Ferreira, A. Pirkle, R. M. Wallace, K. A. Cychocz, M. Thommes, D. Su, E. A. Stach and R. S. Ruoff, *Science*, 2011, **332**, 1537.
97 A. Jänes, L. Permann, M. Arulepp and E. Lust, *Electrochem. Commun.*, 2004, **6**, 313.
98 J. Chmiola, G. Yushin, Y. Gogotsi, C. Portet, P. Simon and P. L. Taberna, *Science*, 2006, **313**, 1760.
99 C. Largeot, C. Portet, J. Chmiola, P.-L. Taberna, Y. Gogotsi and P. Simon, *J. Am. Ceram. Soc.*, 2008, **130**, 2730.
100 A. Kajdos, A. Kvit, F. Jones, J. Jagiello and G. Yushin, *J. Am. Chem. Soc.*, 2010, **132**, 3252.
101 M. Oschatz, E. Kockrick, M. Rose, L. Borchardt, N. Klein, I. Senkovska, T. Freudenberg, Y. Korenblit, G. Yushin and S. Kaskel, *Carbon*, 2010, **48**, 3987.
102 T. A. Centeno, O. Sereda and F. Stoeckli, *Phys. Chem. Chem. Phys.*, 2011, **13**, 12403.
103 X. H. Yang, Y. G. Wang, H. M. Xiong and Y. Y. Xia, *Electrochim. Acta*, 2007, **53**, 752.
104 J. K. Chang, M. T. Lee, C. H. Huang and W. T. Tsai, *Mater. Chem. Phys.*, 2008, **108**, 124.
105 P. Ragupathy, H. N. Vasan and N. Munichandraiah, *J. Electrochem. Soc.*, 2008, **155**, A34.
106 I.-T. Kim, M. Egashira, N. Yoshimoto and M. Morita, *Electrochim. Acta*, 2011, **56**, 7319.
107 H. Wang, T. K.-J. Köster, N. M. Trease, J. Segalini, P.-L. Taberna, R. Simon, Y. Gogotsi and C. P. Grey, *J. Am. Chem. Soc.*, 2011, **133**, 19270.